Applied Catalysis B: Environmental 220 (2018) 202–210

Contents lists available at ScienceDirect

Applied Catalysis B: Environmental

journal homepage: www.elsevier.com/locate/apcatb

Highly porous carbon nitride by supramolecular preassembly of monomers for photocatalytic removal of sulfamethazine under visible light driven

Chengyun Zhou[a,b], Cui Lai[a,b], Danlian Huang[a,b,*], Guangming Zeng[a,b,*], Chen Zhang[a,b], Min Cheng[a,b], Liang Hu[a,b], Jia Wan[a,b], Weiping Xiong[a,b], Ming Wen[a,b], Xiaofeng Wen[a,b], Lei Qin[a,b]

[a] College of Environmental Science and Engineering, Hunan University, Changsha, Hunan 410082, China
[b] Key Laboratory of Environmental Biology and Pollution Control (Hunan University), Ministry of Education, Changsha, Hunan 410082, China

ARTICLE INFO

Keywords:
Carbon doping g-C_3N_4
Photocatalysis
Charge transfer
Sulfamethazine
Water treatment

ABSTRACT

Many organic and inorganic compounds have been developed as visible light driven photocatalysts for environment and energy application. In this work, a metal-free carbon doping–carbon nitride (BCM-C_3N_4) nanocomposite was synthesized by introducing barbituric acid and cyanuric acid during the polymerization of melamine. The BCM-C_3N_4 was characterized by structure, porosity, optical performance, and photoelectrochemical properties. Results demonstrated that BCM-C_3N_4 sample exhibited higher surface area, lower fluorescence intensity, better photocurrent signals and more efficient charge transfer in comparison to pure C_3N_4. The BCM-C_3N_4 exhibits excellent photocatalytic degradation ability of sulfamethazine (SMZ) under visible light irradiation. Much superior photocatalytic activity and high pollutant mineralization rate was achieved by BCM-C_3N_4, where it was 5 times than that of pristine C_3N_4. The effect of initial SMZ concentrations on photocatalyst was also investigated. Additionally, the trapping experiments and electron spin resonance tests demonstrated that the main active species, such as $\cdot O_2^-$ and h^+, could be produced under light irradiation. This work might provide an effective approach to the design of low-cost and highly efficient photocatalysis degradation systems for water treatment.

1. Introduction

Water contaminated by antibiotics is becoming a worldwide environmental issue [1–6]. Potentially negative concerns of these antibiotics active compounds contain abnormal physiological processes, reproductive damage, increased cancer incidences, and enhanced toxicity of chemical mixtures [7,8]. The contaminants are in low concentration at present, but tend to be accumulated in long periods of time. Sulfonamide antibiotics have been detected at concentrations up to 900 mg kg^{-1} in manure, which can be transported to surface water, groundwater and soils. Sulfamethazine (SMZ 4-amino-N-[4,6-dimethyl-2-pyrimidinyl] benzenesulfonamide), which belongs to the sulfonamide group of antibiotics, is commonly used in veterinary industry [9]. Traditional methods, including physical adsorption [10–14], chemical reactions [15,16], and biological degradation [17–20], may be effective for remediation. However, pollutants just transfer from water phase to another phase with these methods, and may cause the secondary pollution if there is no suitable further treatment [21–23].

Semiconductor photocatalysis technique has aroused widespread concern and has been successfully employed to solve the environmental problems [24–28]. Also, it is an economic and environmental technology [29]. The solar photocatalysis process including three steps: (i) light harvest, (ii) photocarrier separation or transport, and (iii) surface reaction [30]. Unfortunately, photocarriers are easy to recombine via the long-distance transportation. To solve the problem and enhance the solar conversion efficiency, the photocarrier transfer kinetics should be accelerated to reach fast separation of the photoexcited electron-hole pairs with novel material or new structural design. Among the numerous photocatalysts, graphic carbon nitride (g-C_3N_4) has gained much interest as an innovative material with desirable visible-light response and medium band gap of 2.7 eV [31,32]. As an earth-abundant, low-cost, biocompatible, and chemically stable photocatalyst, g-C_3N_4 can easily be fabricated from melamine, urea, etc. [33]. It has been developed as a metal-free visible-light sensitive photocatalyst in 2009 and applied in all kinds of photocatalytic branches, such as H_2/O_2 evolution from water splitting [34,35], contaminant degradation [36], CO_2 reduction [37], and so on. However, g-C_3N_4 has a low efficiency under visible light due to the high recombination of photo-generated electron (e^-)-hole (h^+) pairs. Thus, different techniques have been employed to improve the efficiency of g-C_3N_4. One strategy for

* Corresponding authors at: College of Environmental Science and Engineering, Hunan University, Changsha, Hunan 410082, China
E-mail addresses: huangdanlian@hnu.edu.cn (D. Huang), zgming@hnu.edu.cn (G. Zeng).

http://dx.doi.org/10.1016/j.apcatb.2017.08.055
Received 20 May 2017; Received in revised form 31 July 2017; Accepted 16 August 2017
Available online 31 August 2017
0926-3373/

improving the charge carrier separation and photocatalytic efficiency is to dope carbon nitride with heteroatoms [38] or heterojunction [39–41] or metal nanoparticles [42–44].

To date, researchers have reported that nonmetal element doping g-C_3N_4 enhanced visible-light photocatalytic activity, such as doping with P, B, C, Cl, and S [45–48]. For example, Deng et al. prepared P-doped g-C_3N_4 and presented improved photocatalytic activity for the simultaneous removal of Cr(VI) and 2,4-DCP under visible light irradiation [49]. Recently, triazine derivatives doped with melamine through hydrogen bonding led to carbon nitride structures attracted widespread attention owing to its outstanding catalytic and photocatalytic activity. g-C_3N_4 can be easily modified by standard organic protocols such as barbituric acid, which was proposed by Wang et al. [50]. Thomas et al. using dimethyl sulfoxide as a solvent to synthesize C_3N_4 based on the cyanuric acid-melamine (CM) complex, which can exhibited superior photocatalytic activity when compared with the bulk material [51]. Shalom et al. presented hollow carbon nitride structures for degradation of rhodamine B dye, using a CM complex in different solvents as a starting product [52]. Also, Zheng et al. prepared optimized carbon-doped g-C_3N_4 and enhanced the reaction rate for the degradation of phenol and persistent organic pollutants when compared with conventional g-C_3N_4 [53]. Mesoporous carbon nitride was synthesized using different nonionic surfactants by Peer et al. [54]. These results indicated that carbon doped g-C_3N_4 could act as a good catalyst for environment management. However, the weak efficiency of carbon doped g-C_3N_4 may due to the limited surface area (40–60 $m^2\,g^{-1}$) [55,56]. Furthermore, a few studies are concerning the degradation system of the typical organic micropollutants in water such as SMZ via carbon doped g-C_3N_4.

In this work, we report a high-surface area, high-porosity carbon nitrides by a facile one-step approach. This technique using the ethanol as the solvent, taking advantage of both melamine-cyanuric acid and the barbituric acid as monomers to form supramolecular carbon nitride (BCM-C_3N_4) via electrostatic interactions or hydrogen bond. The BET surface area of BCM-C_3N_4 was up to 179 $m^2\,g^{-1}$. With the high surface area and porosity, the synthesized carbon nitrides presented desirable optical properties, and their wide band gap improved visible light absorption, which made them more suitable for photocatalytic applications. The photocatalytic activity was tested by measuring the degradation of SMZ under visible light illumination with the presence of photocatalyst. The chemical structure, morphology, and optical properties of the resulting carbon nitrides were characterized. The performance including degradation efficiency and photocatalytic stability of the photocatalyst under visible light was observed. The effects of initial concentration and the removal rate of total organic carbon were also discussed. The predominant radicals in the photodegradation system were discussed by radicals trapping experiment and electron spin-resonance spectroscopy (ESR) analysis. Meanwhile, a possible degradation pathway of SMZ was proposed. It is anticipated that this metal-free photocatalyst can be a promising candidate for other degradation systems.

2. Experimental

2.1. Materials

Melamine (> 99%), cyanuric acid (> 98%), barbituric acid (> 99%), and Sulfamethazine (> 99%) were purchased from Sinopharm Chemical Reagent Co., Ltd (Shanghai, China). All the reagents and materials were of analytical grade and used as received without additional purification or treatment. De-ionized water (18.25 MΩ.cm) was used in the whole experiment.

2.2. Characterization

The specific surface area, pore volume and pore size of g-C_3N_4, BCM-C_3N_4 were measured by the Brunauer-Emmett-Teller (BET) adsorption method (Micromeritics Instrument Corporation, TRISTAR3020, USA). The photoluminescence (PL) spectra were recorded with Hitachi F-7000 fluorescence spectrophotometer at an excitation wavelength of 365 nm. The UV–vis diffuse reflectance spectra (DRS) were performed on a UV–vis spectrophotometer (Cary 300, USA) with an integrating sphere. The crystal phase of the samples was determined by a D/max-2500 X-ray diffractometer (XRD; Rigaku, Japan) using Cu $K\alpha$ radiation (λ = 0.15406 nm) in the region of 2θ from 10° to 80°. X-ray photoelectron spectrum (XPS) of the samples was obtained by using an ESCALAB 250Xi spectrometer (Thermo Fisher, USA) with Al $K\alpha$ radiation ($h\nu$ = 1486.6 eV). Their morphology was examined by transmission electron microscope (TEM, JEOL JEM-2100F). The light irradiation source was a 300 W Xe arc lamp (CEL-HXF300, Beijing). The visible light used in this study was obtained by cutting UV light (λ < 420 nm) with a filter (Beijing China Education Au-light Co., Ltd). The total organic carbon (TOC) was applied to analyze the mineralization degree of organic contaminants on Analytik Jena AG (Multi N/C 2100).

2.3. Preparation of samples

2.3.1. Synthesis of g-C_3N_4

In a typical synthesis process, 10 g of melamine was placed into a ceramic crucible with a cover and then loaded into the central region of a muffle furnace. The crucible was firstly heated to 550 °C with a heating rate of 2.3 °C min^{-1} and maintained at 550 °C for 4 h, and then cooled down naturally. After cooling to ambient temperature, the obtained yellow agglomerate (g-C_3N_4) was ground into powder.

2.3.2. Synthesis of BCM-C_3N_4

The BCM-C_3N_4 was prepared from melamine, cyanuric acid, and barbituric acid by modified method [57,58]. 5.0 g of melamine, 5.0 g of cyanuric acid, and 0.5 g of barbituric acid were first dispersed in 100 mL of ethanol to form suspension. The suspension was next stirred at ambient temperature for 2 h, followed by sonication at room temperature for an additional 1 h. The suspension was then dried on a hot plate at 90 °C until no obvious liquid found. The calcination procedure was exhibited in the part of 2.3.1. For comparison, CM-C_3N_4 sample was obtained without barbituric acid.

2.4. Photodegradation evaluation

The photodegradation activities of obtained samples were investigated via the degradation of SMZ in aqueous solution under a 300W Xe lamp in an aqueous solution under visible light (> 420 nm). In photocatalytic degradation experiment, 50 mg of powder photocatalyst was dispersed into 50 mL of SMZ (10 mg L^{-1}) solution. Before illumination, the suspensions were stirred in dark for 1 h to reach the adsorption-desorption equilibrium. After that, the mixture solutions were illuminated under visible light. At a given time interval of irradiation, aliquots were separated from the suspension. The SMZ concentration was determined using an HPLC Series 1100 (Agilent, Waldbronn, Germany) equipped with a UV–vis detector. The Column was C-18 column (4.6 × 250 mm) at the temperature of 30 °C. The mobile phase was water–acetonitrile (80:20, v/v) with 0.1% acetic acid at the flow rate of 1 mL min^{-1}. The sample volumes for injection were all 20 μL and the wavelength of detector was 270 nm.

2.4.1. Photoelectrochemical measurement

Photoelectrochemcial tests were carried out on a CHI 660D workstation in a three-electrode model, utilizing a Pt electrode (40 × 0.55 mm, 99%) as the counter electrode and an Ag/AgCl electrode as the reference electrode. A 300 W Xe lamp was used as a light source. Typically, the working electrodes were prepared as follows: 10 mg of the photocatalyst was suspended in 1 mL of 0.5% nafion

Table 1
surface area and pore volume for g-C_3N_4 and BCM-C_3N_4.

Samples	Surface area($m^2\ g^{-1}$)	Pore volume ($cm^3\ g^{-1}$)
g-C_3N_4	13.55	0.05
BCM-C_3N_4	179.03	0.56

solution to make slurry. Then, 100 μL of the slurry dropped onto a 1 cm × 2 cm FTO slice with an effective working area of 1 cm^2. The electrochemical impedance spectroscopy (EIS) was performed in 100 mL of 0.2 M Na_2SO_4 aqueous solution with the above three-electrode system.

2.5. Active species trapping experiment

The active species trapping were ethylenediaminetetraacetic acid disodium salt (EDTA-2Na), benzoquinone (BQ), and isopropanol (IPA), which were introduced as the scavengers to detect holes (h^+), superoxide radicals ($\cdot O_2^-$) and hydroxyl radicals ($\cdot OH$), respectively. The experiment was analyzed by 1 mM scavengers to degrade SMZ in an aqueous solution under visible light (> 420 nm) (Table 1).

3. Results and discussion

3.1. Crystal structure and morphology

Direct evidence for the g-C_3N_4 formation was obtained by FT-IR spectroscopy, XRD, and XPS. The FT-IR spectra of g-C_3N_4, CM-C_3N_4, and BCM-C_3N_4 were shown in Fig. 1. According to the FT-IR spectrum of g-C_3N_4, several bands in the 1200–1700 cm^{-1} region are attributed to the typical stretching vibrations of C—N heterocycles. The peak at 805 cm^{-1} belongs to the triazine. These results are highly consistent with the previous reports [59].

The XRD patterns of g-C_3N_4, CM-C_3N_4, and BCM-C_3N_4 were also investigated, and the results were depicted in Fig. 2. All samples had a similar XRD pattern which could be ascribed to a typical graphite-like structure. The peak of g-C_3N_4 at 13.1° is ascribed to the (100) inplanar ordering of tri-s-triazine units. The strong interplanar stacking peak at 27.2° corresponding to the (002) interlayer stacking. Compared to the g-C_3N_4, the (100) peak of BCM-C_3N_4 is significantly weakened, which is a feature of BCM-C_3N_4 with mesoporous structure. Also, the (002) peak of BCM-C_3N_4 obviously became weaker and broader, which was ascribed to the addition of cyanuric acid and/or barbituric acid [60].

XPS test results of C, N, and O for g-C_3N_4 and BCM-C_3N_4 were presented in Fig. 3. The survey of BCM-C_3N_4 displayed that the

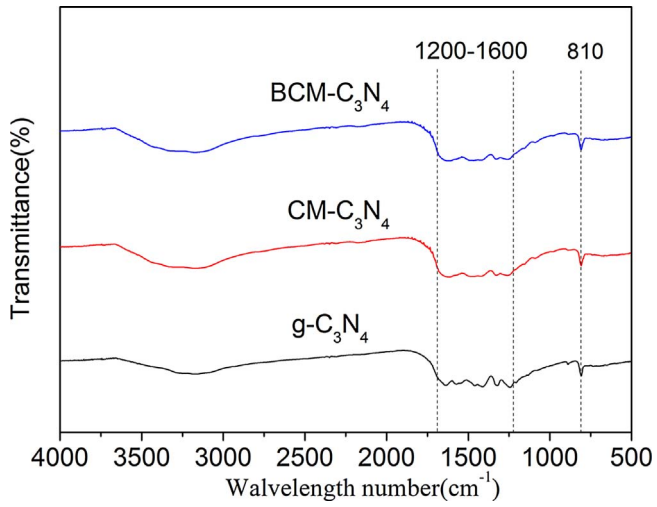

Fig 1. The FT-IR analysis of g-C_3N_4, CM-C_3N_4, and BCM-C_3N_4.

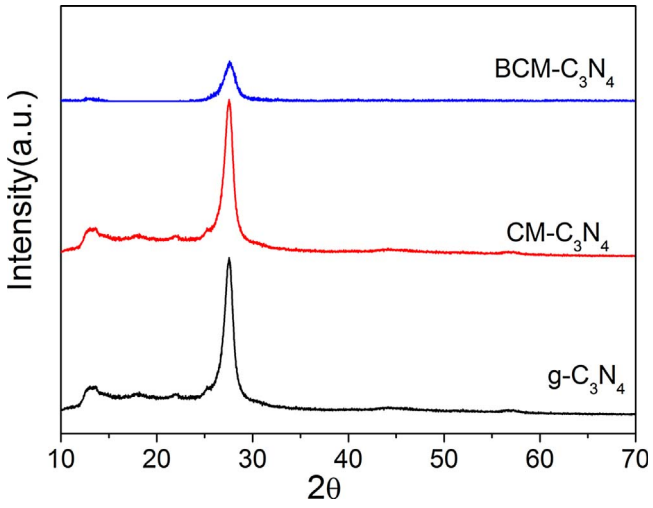

Fig. 2. The XRD pattern of g-C_3N_4, CM-C_3N_4, and BCM-C_3N_4.

elements of the samples were C, N, and O. The C1 s binding energy region (284.9 eV) was ascribed to alkyl carbon (C═C—C or C—H), most likely either adventitious carbon adsorbed on the surface or any sp^3 graphitic carbon formed during pyrolysis. The peak at 288.4 eV was attributed to the signals of sp^2 carbon (N—C═N) presented in the backbone of g-C_3N_4. These signals are usually observed in the XPS spectrum of carbon nitrides. The N 1 s peak at 398.8 ± 0.2 eV and 404.1 ± 0.2 eV correspond to sp^2 hybridized aromatic N in tri-ring (C—N═C) and positively charged localization, respectively. The peak with a high binding energy at 399.7 ± 0.1 eV is assigned to nitrogen (N-$(C)_3$) at the structural edges of g-C_3N_4. The peak located at 400.9 ± 0.1 indicated the presence of amino functions (C—N—H), originating from the terminal amino groups on the surface [61]. As for O 1 s spectrum, it exhibited the predominant characteristic peak at 529.9 eV. As shown in Table S1, the surface atomic ratio from XPS revealed that the C/N molar ratio of the BCM-C_3N_4 nanosheet (0.67) was much smaller than that of the g-C_3N_4 (0.94), indicating the presence of surface carbon vacancies in the BCM-C_3N_4 nanosheet. The above results were consistent with the previous reports, confirming the successful of preparation of g-C_3N_4 [62].

The morphological of g-C_3N_4 and BCM-C_3N_4 have been characterized by the TEM images. As shown in Fig. 4a and b, the pristine g-C_3N_4 presented stacked sheets structure and smooth surface. After addition of the barbituric acid and cyanuric acid, the BCM-C_3N_4 obviously displayed thin nanosheet structures and randomly distributed mesopores, which significantly differed from the mainly dense and stacked sheets of the pristine g-C_3N_4 (Fig. 4c). As shown in Fig. 4d, many pores, approximately 5–10 nm, were embedded in a porous BCM-C_3N_4. These surface pores existed on BCM-C_3N_4 can provide a lot of active sites and improve mass transportation, which can be further utilized for photocatalytic degradation.

To further study the surface morphology and pore volume in the as-prepared samples, the nitrogen adsorption-desorption isotherms experiments have been performed in Fig. S1 and Table 2. The BET surface area and pore volume of BCM-C_3N_4 were calculated to be 179.03 $m^2\ g^{-1}$ and 0.56 $cm^3\ g^{-1}$, respectively. Photodegradation is a surface reaction. The increase surface area and pore volume may offer more active sites for the pollutants, enhancing its photocatalytic efficiency. The results mentioned above as supported by the TEM and further demonstrate the successful preparation of BCM-C_3N_4 which possesses nanosheet structure with pores on the surface [63,64].

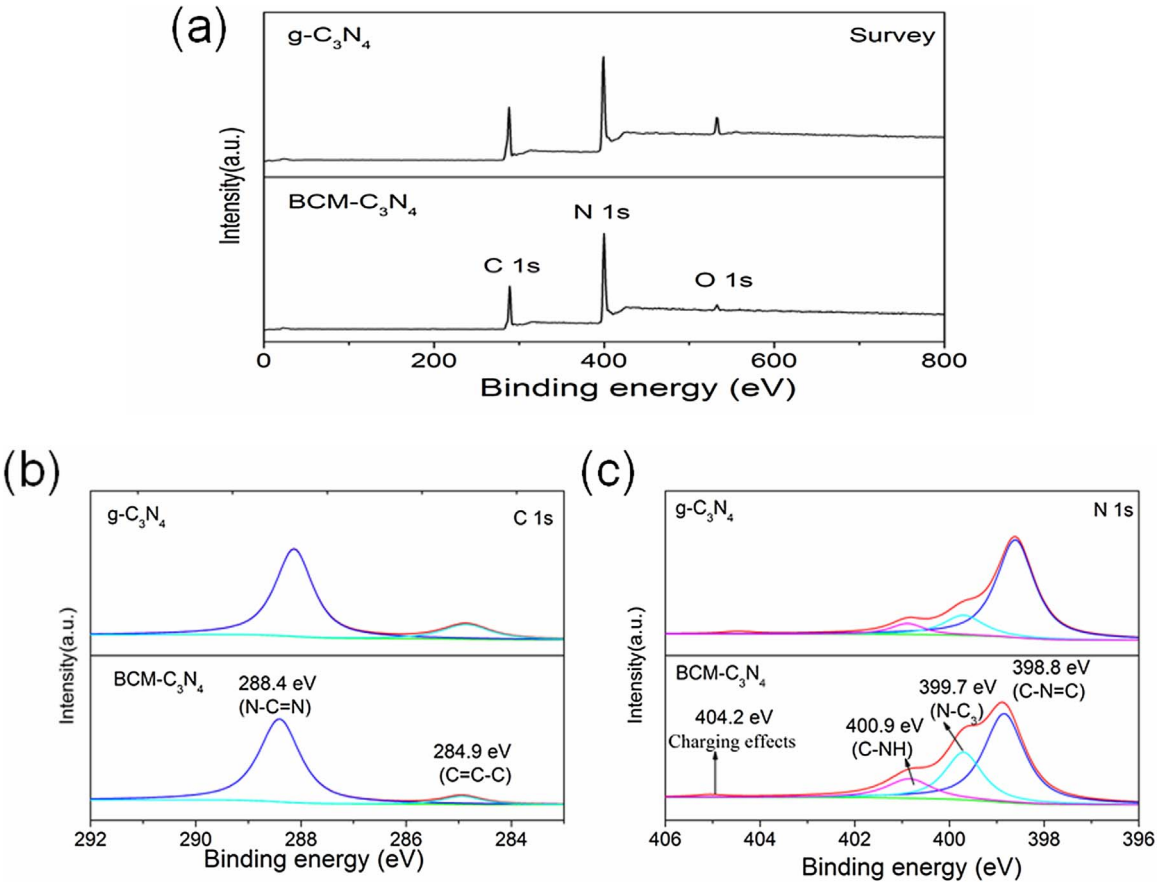

Fig. 3. The XPS spectra of g-C_3N_4 and BCM-C_3N_4: (a) survey spectra, (b) high resolution C 1s, and (c) high resolution N 1s.

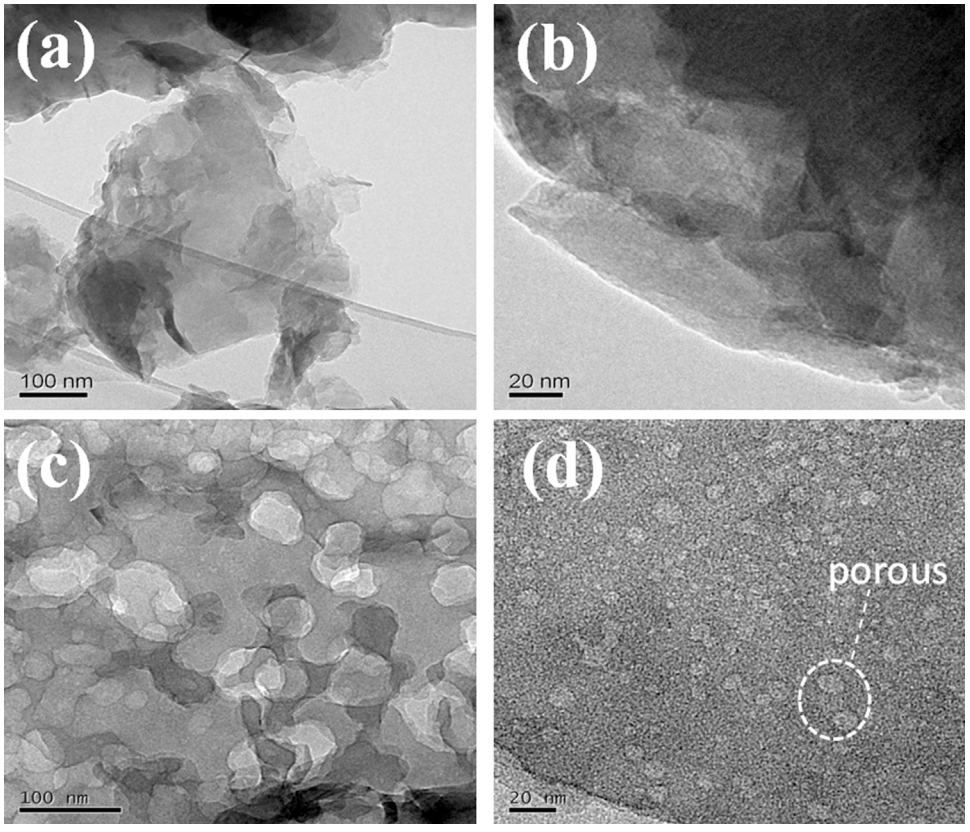

Fig. 4. TEM images of as-prepared photocatalysts: (a) low and (b) high resolution of g-C_3N_4, (c) low and (d) high resolution of BCM-C_3N_4.

Table 2
Dynamics analysis of emission decay for the different samples.

Samples	A1 (%)	τ1 (ns)	A2 (%)	τ2(ns)
g-C_3N_4	45.98	2.14	54.02	7.45
BCM-C_3N_4	48.63	1.48	51.37	5.11

3.2. Optical property, photoluminescence, and photo electrochemical properties

DRS were used to study the optical absorption properties of the g-C_3N_4, CM-C_3N_4, and BCM-C_3N_4 samples. As shown in Fig. 5a, g-C_3N_4 has an adsorption at 453 nm which fitted with the previous report [65]. After doping the barbituric acid and cyanuric acid with melamine, the absorption edge gradually moved to longer edge, which can significantly enhance the visible light absorption. The energy band gap of semiconductors can be determined from the intercept of the tangents to the plots of $(\alpha h\nu)^2$ *versus* $h\nu$ [66]. As presented in Fig. 5b, we can obtain that the band gap of CM-C_3N_4 and BCM-C_3N_4 are 2.32 eV and 2.02 eV, respectively, which are narrower than the g-C_3N_4 (2.68 eV). The carbon doping of BCM-C_3N_4 could change its band gap obviously. Furthermore, the conduction band and valence band of the samples could be calculated by the equation as following [67]:

$$E_{CB} = X\text{-}E_C\text{-}1/2E_g \quad (1)$$

$$E_{VB} = E_{CB} + E_g \quad (2)$$

Where X is the eletronegativity of the semiconductor, and the value for g-C_3N_4 is 4.72 eV, E_C is the energy of free electrons on the hydrogen scale (about 4.5 eV vs NHE). According the data above, the E_{CB} and E_{VB} of BCM-C_3N_4 are calculated to be −0.79 eV and +1.23 eV, respectively. The E_{CB} and E_{VB} of g-C_3N_4 are calculated to be −1.12 eV and +1.56 eV, respectively.

To confirm the photo-response ability and photogenerated charges recombination efficiency in the photocatalyst, the transient photocurrent measurement was introduced. As shown in Fig. 5c, it can be seen that all the electrodes exhibited rapid and stable photocurrent response under light illumination. The transient photocurrent of BCM-C_3N_4 increased by 2.5 times compared to pristine g-C_3N_4. Large enhancement of transient photocurrent in the BCM-C_3N_4 sample was indeed observed, indicating that the better separation of photogenerated charges carriers and more efficient electron transportation at the interfaces. EIS is another method to explain the electron-transfer efficiency at the electrodes. Fig. 5d presented an overview of the semicircular Nyquist plots for the samples, and g-C_3N_4 showed the bigger diameter, which implied that the poor electrical conductivity may inhibit the electron transfer. The BCM-C_3N_4 shows smaller arc radius than g-C_3N_4, which could be attributed to the doping of barbituric acid.

PL was measured to study the separation efficiency of photogenerated charge carriers of as-fabricated semiconductor photocatalyst. The samples were excited by the wavelength of 360 nm, because the light in this wavelength could initiate both the bandgap transition of photocatalyst. The PL intensities of BCM-C_3N_4 are found to be greatly lowered in comparison with that of g-C_3N_4 in Fig. 6a, which reflect the charge carrier may be suppressed by doping cyanuric acid and barbituric acid.

For better understanding the process of charge separation and transfer in the samples, fluorescence decay time was provided. As shown in Fig. 6b, the change in the tendency of decay time can be determined. It could be clearly seen that, when cyanuric acid and barbituric acid were integrated with the pristine g-C_3N_4, the emission lifetime of BCM-C_3N_4 was decreased from 7.45 ns to 5.12 ns (shown in Table 2). The reduced decay lifetime and quenched PL suggest more effective charge-carrier formation and faster interfacial charge transfer occurring in the doping photocatalyst due to the emergence of non-

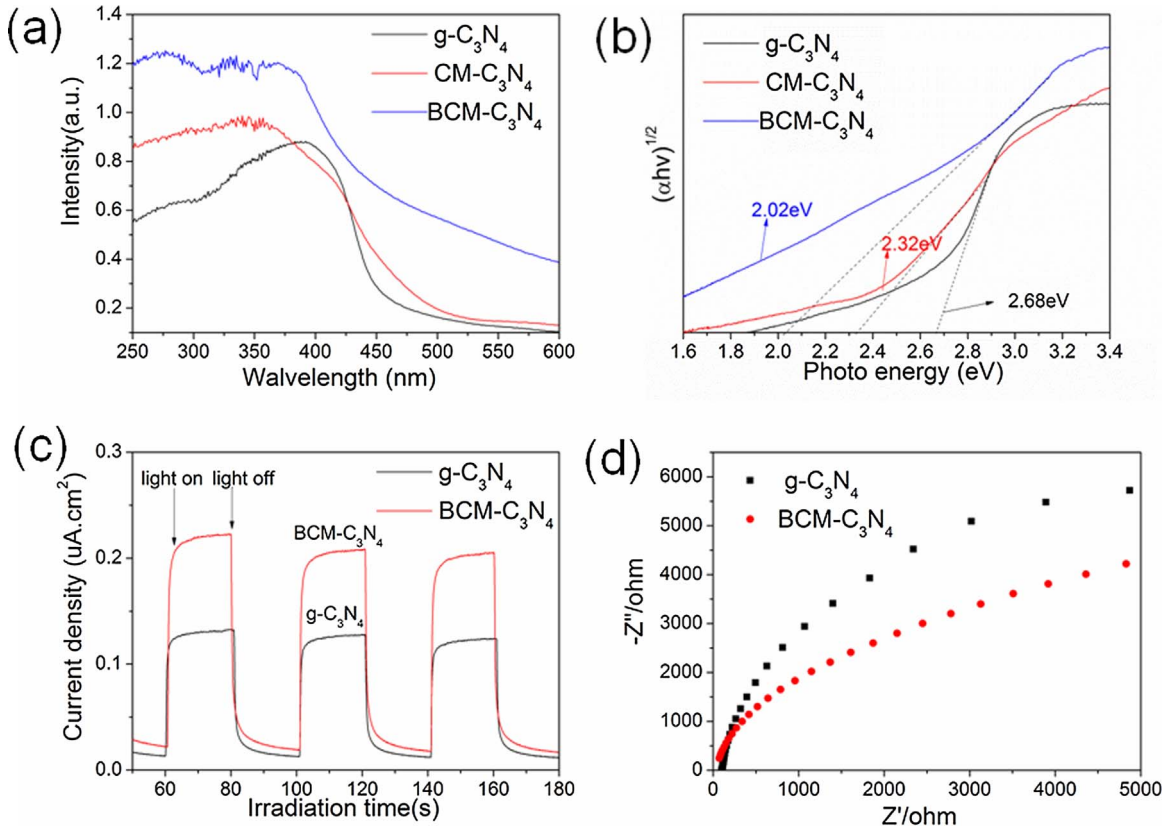

Fig. 5. (a) UV–vis adsorption spectra and digital photograph of the as-prepared samples, (b) the plots of $(\alpha h\nu)^{1/2}$ *vs* photon energy $(h\nu)$, (c)transient photocurrent response for the samples, and (d) the EIS for the samples.

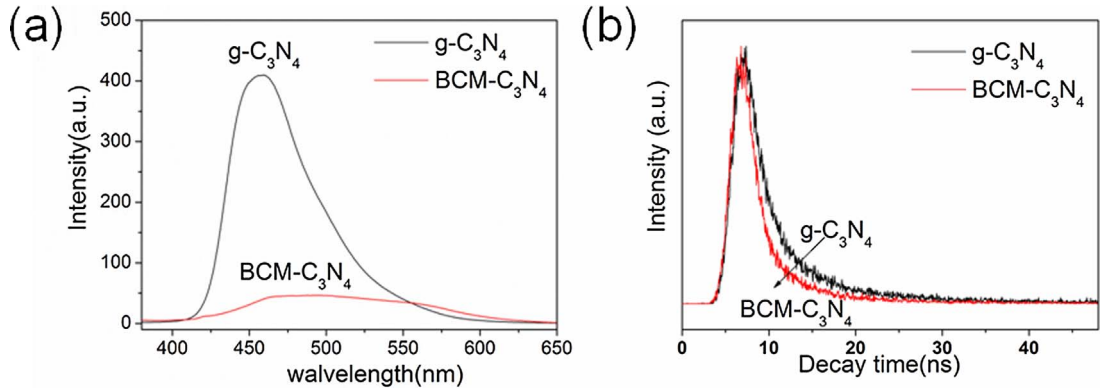

Fig. 6. (a) photoluminescence (PL) spectra and (b) the fitting curves of fluorescence decay of samples.

radiative quenching pathways.

3.3. Photocatalytic activity and photocatalyst stablity

The photocatalytic activities of as-prepared g-C_3N_4, CM-C_3N_4, and BCM-C_3N_4 samples composites were evaluated by the decomposition of the micropollutant SMZ under visible light irradiation. Before irradiation, the dark adsorption test was carried out. The adsorption efficiency of samples was added in Table S1. There was no obvious increase of adsorption for all the samples after 60 min dark reaction. As revealed in Fig. 7a, when all the samples were exposed to visible light, the BCM-C_3N_4 showed a photocatalytic degradation rate over 90% for SMZ. However, the degradation rate of pristine g-C_3N_4 was 20%, which was the lowest removal efficiency among those there photocatalysts. It suggested that BCM-C_3N_4 showed excellent photocatalytic performance, which may due to the high efficient of photoinduced electron-hole pairs separation.

Different initial concentrations of SMZ (5–100 mg L^{-1}) were also applied to test the activities of the photocatalysts (Fig. 7b). With the increasing concentration, the removal efficiency was decreased from 98% (5 mg L^{-1}) to 22% (100 mg L^{-1}) in 1 h. This negative effect explained that a higher concentration of SMZ would decrease the photon adsorption on catalyst. The results indicated that lower SMZ concentration was more beneficial to gain higher removal efficiency. Also, in the practical wastewater treatment, dilution was essential in the process of pretreatment.

The ability to deep mineralize organic pollutants is crucial for environmental governance. In this work, the mineralization for SMZ could be measured by TOC analysis. As shown in Fig. 7c, the removal efficiency of TOC in SMZ aqueous solution was slower than that of SMZ decomposition, about 60% of TOC could be removed for 2 h visible light irradiation. The result demonstrated that BCM-C_3N_4 exhibited superior photocatalytic activity in the SMZ degradation with a favorable mineralization ability.

To discuss the stability of BCM-C_3N_4, the sample had been performed four reaction runs under the same conditions. For each cycle, the catalyst was collected after the centrifugation, washing, and drying for the next test. Compare fresh BCM-C_3N_4 with aged BCM-C_3N_4, little inhibition was observed in SMZ degradation. As presented in Fig. 7d, photodegradation efficiencies of SMZ solution exhibited no obvious reduction, even after four circles. To further demonstrate the stability of the BCM-C_3N_4, the FT-IR and XRD of the fresh and used samples have been provided for comparison in Fig. S2 and Fig. S3.

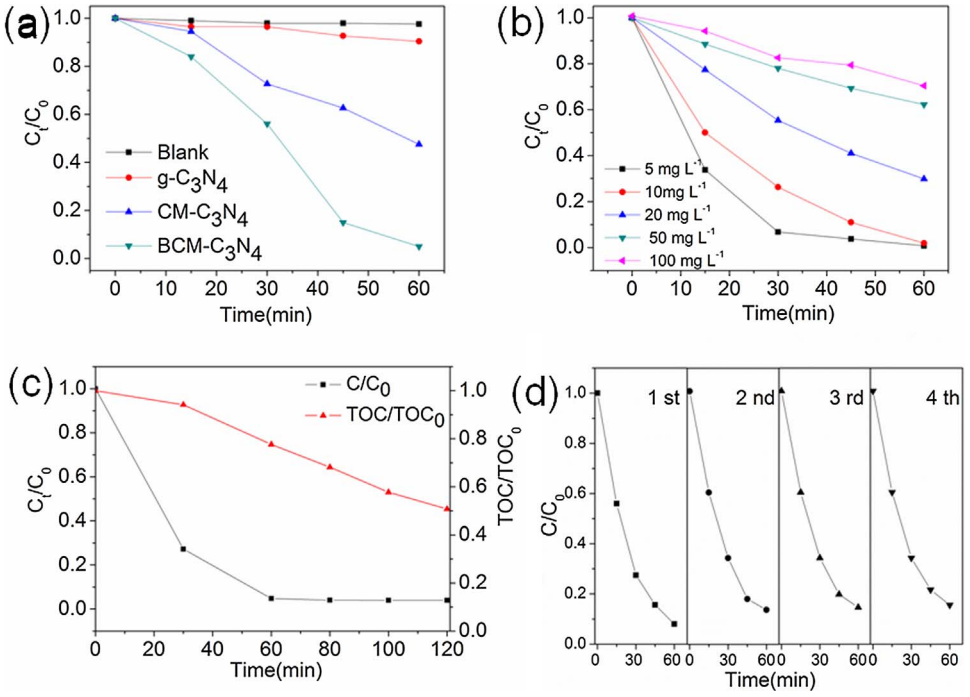

Fig. 7. (a) Photodegradation rate of SMZ on different photocatalyst samples, (b) effect of initial concentration of SMZ on BCM-C_3N_4, (c) The photodegradation and TOC removal curves of SMZ on BCM-C_3N_4, and (d) The cycling runs in the photodegradation of SMZ over BCM-C_3N_4 under visible light irradiation (> 420 nm).

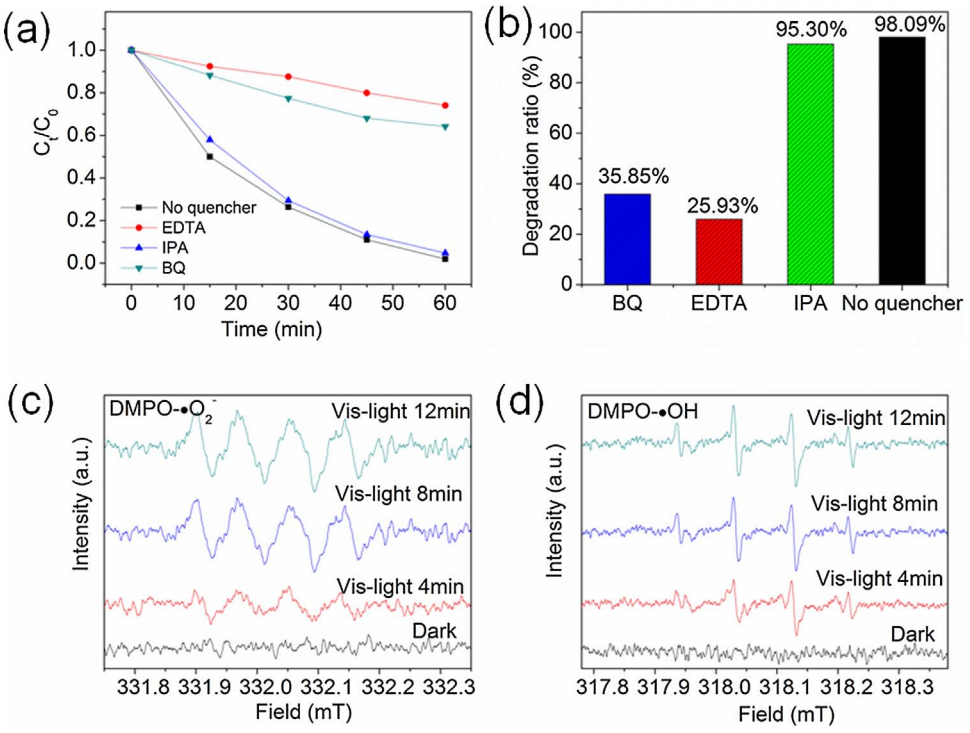

Fig. 8. The photocatalytic degradation plots of SMZ over BCM-C_3N_4 (a, b) with the addition of hole, $\cdot O_2^-$ and ·OH radical scavenger under visible light irradiation and ESR spectra of radical adducts trapped by DMPO in the BCM-C_3N_4 dispersion under both the dark and visible light irradiation (> 420 nm) condition: (c) in methanol dispersion for DMPO-$\cdot O_2^-$; (d) in aqueous dispersion for DMPO-·OH.

3.4. Degradation mechanism of BCM-C_3N_4

To identify main reactive species involved in photocatalytic degradation process, scavenger tests were conducted. ethylenediaminetetraacetic acid disodium (EDTA-2Na), 1,4-Benzoquinone (BQ), and isopropanol (IPA), were adopted as the scavengers of hole (h^+), super oxide radical($\cdot O_2^-$), and hydroxyl radical (·OH), respectively [68,69]. As depicted in Fig. 8a and 8b, it is obvious that the photocatalytic performance decrease after adding the EDTA-2Na or BQ. The activity was inhibited by 1 mM EDTA-2Na and the degradation rate of SMZ decreased from 98.09% to 25.93%. This result suggested that EDTA-2Na acts as h^+ scavenger, which will consume the reactive species and further reduce the activity of BCM-C_3N_4. With the addition of BQ, the photocatalytic activity of BCM-C_3N_4 decreased from 98.09% to 35.85%, which implies the $\cdot O_2^-$ was also the major species in the degradation of SMZ. However, in the presence of IPA, the photodegradation rate of SMZ exhibited no obvious decrease, revealing that ·OH active species were the minor factor in the photocatalytic reaction. Based on the above results, it could be deduced that the h^+, $\cdot O_2^-$, and ·OH played an important role in the photodegradation of BCM-C_3N_4.

To further confirm the reactive oxygen species evolved in the photocatalysis over BCM-C_3N_4 nanocomposite, the ESR with 5,5-dimethyl-1-pyrroline N-oxide (DMPO) in aqueous solution was performed [39]. As shown in Fig. 8c, four obvious signals with BCM-C_3N_4 in methanol were produced, which could be assigned to DMPO-$\cdot O_2^-$ under light illumination. There is no $\cdot O_2^{--}$ signal in the dark, but an increasing signal of DMPO-$\cdot O_2^{--}$ could be observed with visible light irradiation. Moreover, the signal of ·OH was also detected in DMPO system when exposed to light in Fig. 8d. The scavenger test and ESR result confirmed that $\cdot O_2^-$and ·OH exist in the BCM-C_3N_4 system under visible light irradiation.

On the basis of the above results, a possible mechanism is proposed to explain the high photocatalytic activity of the as-prepared BCM-C_3N_4 in Fig. 9. BCM-C_3N_4 has higher specific surface area and numerous active sites for the reaction process. Under visible light irradiation, the BCM-C_3N_4 could generate electrons and holes. The electrons on the CB of BCM-C_3N_4 (-0.79 eV), which are more negative than E ($O_2/\cdot O_2^-$) (−0.33 eV), are a good reductant that could efficiently reduce oxygen molecules adsorbed on the surface of the photoanode to $\cdot O_2^-$. Moreover, super-oxide radicals $\cdot O_2^-$ are the most important oxidizing species and then induces the SMZ degradation. The standard redox potential of $\cdot OH/OH^-$ is +2.38 eV, which is more positive than the VB position of BCM-C_3N_4 (+1.23 eV). Thus, the photogenerated hole (h^+) cannot react with H_2O to produce ·OH over BCM-C_3N_4 nanosheet. The generated ·OH may attributed to the conversion of the $\cdot O_2^-$. In conclusion, the predominant active species ($\cdot O_2^-$ and h^+) as well as the converted products (·OH) could effectively degrade SMZ into CO_2 and H_2O, etc. According to the above analysis, the reaction process can be list as following equations:

$$\text{BCM-}C_3N_4 + h\nu \rightarrow \text{BCM-}C_3N_4\ (h^+ + e^-) \quad (3)$$

$$O_2 + e^- \rightarrow \cdot O_2^- \quad (4)$$

$$\cdot O_2^- + e^{--} + 2H^+ \rightarrow H_2O_2 \quad (5)$$

$$H_2O_2 + e^- \rightarrow OH^- + \cdot OH \quad (6)$$

$$(\cdot O_2^-, h^+ \text{ and } \cdot OH) + \text{SMZ} \rightarrow \text{degradation products } (CO_2 + H_2O) \quad (7)$$

4. Conclusion

In conclusion, a visible light driven mesoporous catalyst has been successfully prepared via carbon doping and thermal process. We have shown that the optical and electronic properties of carbon nitride polymer can be easily modified by nonmetal doping. Under visible light irradiation, the BCM-C_3N_4 composite could remove 98% of SMZ in 1 h, which was more efficient than that of pristine C_3N_4 (removed 20% of SMZ in 1 h). The PL, transient photocurrent, and fluorescence decay time studies revealed that effective electron–hole separation in the excited state made it an effective photocatalyst. The active species $\cdot O_2^-$, h^+ and ·OH were produced and were deduced by scavenger tests and ESR in the catalyst system. Furthermore, the visible light photoactivity of the as-prepared photocatalyst under different pollutant concentration was also investigated. The study may provide new insight into the strategies for the design and utilization of highly efficient and

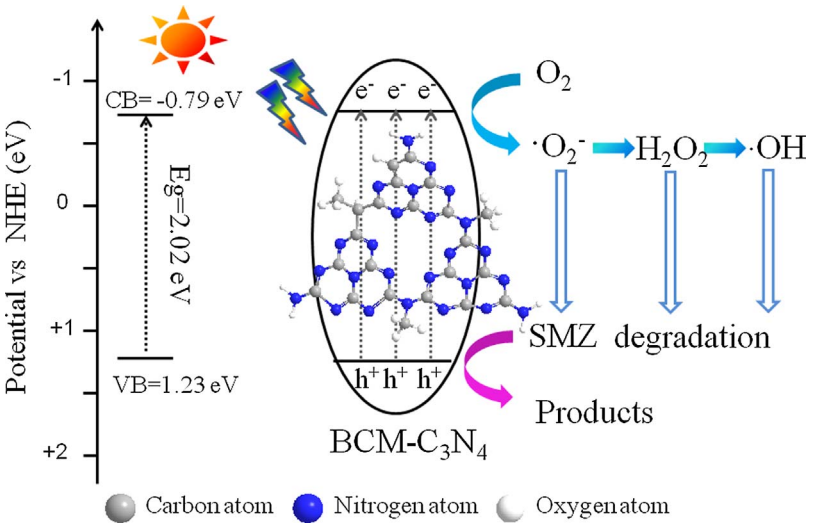

Fig. 9. A schematic illustration of degradation of SMZ on BCM-C_3N_4 under visible light irradiation.

stable non-metal photocatalyst for visible light driven degradation of pollutants.

Acknowledgements

This study was financially supported by the Program for the National Natural Science Foundation of China (51521006, 51579098, 51378190, 51408206), the National Program for Support of Top-Notch Young Professionals of China (2014), the Fundamental Research Funds for the Central Universities, Hunan Provincial Science and Technology Plan Project (No. 2016RS3026), the Program for New Century Excellent Talents in University (NCET-13-0186), the Program for Changjiang Scholars and Innovative Research Team in University (IRT-13R17).

Appendix A. Supplementary data

Supplementary data associated with this article can be found, in the online version, at http://dx.doi.org/10.1016/j.apcatb.2017.08.055.

References

[1] G. Zeng, M. Chen, Z. Zeng, Nature 499 (2013) 154.
[2] G. Zeng, M. Chen, Z. Zeng, Science 340 (2013) 1403.
[3] Y. Feng, J.-L. Gong, G.-M. Zeng, Q.-Y. Niu, H.-Y. Zhang, C.-G. Niu, J.-H. Deng, M. Yan, Chem. Eng. J. 162 (2010) 487–494.
[4] T. Fan, Y. Liu, B. Feng, G. Zeng, C. Yang, M. Zhou, H. Zhou, Z. Tan, X. Wang, J. Hazard. Mater. 160 (2008) 655–661.
[5] D. Huang, W. Xue, G. Zeng, J. Wan, G. Chen, C. Huang, C. Zhang, M. Cheng, P. Xu, Water Res. 106 (2016) 15–25.
[6] L. Qin, G. Zeng, C. Lai, D. Huang, C. Zhang, P. Xu, T. Hu, X. Liu, M. Cheng, Y. Liu, Sens. Actuators B: Chem. 243 (2017) 946–954.
[7] S. Zhong, C. Zhou, X. Zhang, H. Zhou, H. Li, X. Zhu, J. Hazard. Mater. 276 (2014) 58–65.
[8] C. Zhou, H. Li, H. Zhou, H. Wang, P. Yang, S. Zhong, J. Sep. Sci. 38 (2015) 1365–1371.
[9] C. Zhang, C. Lai, G. Zeng, D. Huang, C. Yang, Y. Wang, Y. Zhou, M. Cheng, Water Res. 95 (2016) 103–112.
[10] P. Xu, G.M. Zeng, D.L. Huang, C.L. Feng, S. Hu, M.H. Zhao, C. Lai, Z. Wei, C. Huang, G.X. Xie, Z.F. Liu, Sci. Total Environ. 424 (2012) 1–10.
[11] J.-L. Gong, B. Wang, G.-M. Zeng, C.-P. Yang, C.-G. Niu, Q.-Y. Niu, W.-J. Zhou, Y. Liang, J. Hazard. Mater. 164 (2009) 1517–1522.
[12] Y. Zhang, G.-M. Zeng, L. Tang, D.-L. Huang, X.-Y. Jiang, Y.-N. Chen, Biosens. Bioelectron. 22 (2007) 2121–2126.
[13] Y. Cheng, H. He, C. Yang, G. Zeng, X. Li, H. Chen, G. Yu, Biotechnol. Adv. 34 (2016) 1091–1102.
[14] X.-J. Hu, J.-S. Wang, Y.-G. Liu, X. Li, G.-M. Zeng, Z.-L. Bao, X.-X. Zeng, A.-W. Chen, F. Long, J. Hazard. Mater. 185 (2011) 306–314.
[15] M. Cheng, G. Zeng, D. Huang, C. Lai, P. Xu, C. Zhang, Y. Liu, J. Wan, X. Gong, Y. Zhu, J. Hazard. Mater. 312 (2016) 184–191.
[16] D.-L. Huang, R.-Z. Wang, Y.-G. Liu, G.-M. Zeng, C. Lai, P. Xu, B.-A. Lu, J.-J. Xu, C. Wang, C. Huang, Environ. Sci. Pollut. Res. 22 (2015) 963–977.
[17] L. Tang, G.-M. Zeng, G.-L. Shen, Y.-P. Li, Y. Zhang, D.-L. Huang, Environ Sci. Technol. 42 (2008) 1207–1212.
[18] D.-L. Huang, G.-M. Zeng, C.-L. Feng, S. Hu, X.-Y. Jiang, L. Tang, F.-F. Su, Y. Zhang, W. Zeng, H.-L. Liu, Environ Sci. Technol. 42 (2008) 4946–4951.
[19] C. Yang, H. Chen, G. Zeng, G. Yu, S. Luo, Biotechnol. Adv. 28 (2010) 531–540.
[20] D. Huang, L. Liu, G. Zeng, P. Xu, C. Huang, L. Deng, R. Wang, J. Wan, Chemosphere 174 (2017) 545–553.
[21] M. Cheng, G. Zeng, D. Huang, C. Lai, P. Xu, C. Zhang, Y. Liu, Chem. Eng. J. 284 (2016) 582–598.
[22] D. Huang, C. Hu, G. Zeng, M. Cheng, P. Xu, X. Gong, R. Wang, W. Xue, Sci. Total Environ. 574 (2017) 1599–1610.
[23] C. Zhang, G. Zeng, D. Huang, C. Lai, C. Huang, N. Li, P. Xu, M. Cheng, Y. Zhou, W. Tang, RSC Adv. 4 (2014) 55511–55518.
[24] Y. Song, J. Tian, S. Gao, P. Shao, J. Qi, F. Cui, Appl. Catal. B: Environ. 210 (2017) 88–96.
[25] Y.-Q. Gao, N.-Y. Gao, Y. Deng, Y.-Q. Yang, Y. Ma, Chem. Eng. J. 195–196 (2012) 248–253.
[26] C. Guo, J. Xu, S. Wang, Y. Zhang, Y. He, X. Li, Catal. Sci. Technol. 3 (2013) 1603.
[27] C. Lai, M.-M. Wang, G.-M. Zeng, Y.-G. Liu, D.-L. Huang, C. Zhang, R.-Z. Wang, P. Xu, M. Cheng, C. Huang, Appl. Surf. Sci. 390 (2016) 368–376.
[28] M. Cheng, G. Zeng, D. Huang, C. Lai, C. Zhang, Y. Liu, Chem. Eng. J. 384 (2017) 98–113.
[29] X. Liu, N. Chen, Y. Li, D. Deng, X. Xing, Y. Wang, Sci. Rep. 6 (2016) 39531.
[30] W. Che, W. Cheng, T. Yao, F. Tang, W. Liu, H. Su, Y. Huang, Q. Liu, J. Liu, F. Hu, Z. Pan, Z. Sun, S. Wei, J. Am. Chem. Soc. 139 (2017) 3021–3026.
[31] D. Tang, G. Zhang, Appl. Surf. Sci. 391 (2017) 415–422.
[32] D. Lu, G. Zhang, Z. Wan, Appl. Surf. Sci. 358 (2015) 223–230.
[33] D. Masih, Y. Ma, S. Rohani, Appl. Catal. B: Environ. 206 (2017) 556–588.
[34] D. Zheng, X.-N. Cao, X. Wang, Angew. Chem. Int. Ed. 55 (2016) 11512–11516.
[35] Y. Zheng, L.H. Lin, B. Wang, X.C. Wang, Angew. Chem. Int. Ed. 54 (2015) 12868–12884.
[36] W. Chen, Y.-X. Hua, Y. Wang, T. Huang, T.-Y. Liu, X.-H. Liu, J. Catal. 349 (2017) 8–18.
[37] S.W. Cao, J.X. Low, J.G. Yu, M. Jaroniec, Adv. Mater. 27 (2015) 2150–2176.
[38] J. Wen, J. Xie, X. Chen, X. Li, Appl. Surf. Sci. 391 (2017) 72–123.
[39] F. Chen, Q. Yang, Y. Wang, J. Zhao, D. Wang, X. Li, Z. Guo, H. Wang, Y. Deng, C. Niu, G. Zeng, Appl. Catal. B: Environ. 205 (2017) 133–147.
[40] J. Wang, L. Tang, G. Zeng, Y. Deng, Y. Liu, L. Wang, Y. Zhou, Z. Guo, J. Wang, C. Zhang, Appl. Catal. B: Environ. 209 (2017) 285–294.
[41] J. Xia, M. Ji, J. Di, B. Wang, S. Yin, Q. Zhang, M. He, H. Li, Appl. Catal. B: Environ. 191 (2016) 235–245.
[42] J. Wang, L. Tang, G. Zeng, Y. Liu, Y. Zhou, Y. Deng, J. Wang, B. Peng, ACS Sustain. Chem. Eng. 5 (2017) 1062–1072.
[43] F. Chen, Q. Yang, J. Sun, F. Yao, S. Wang, Y. Wang, X. Wang, X. Li, C. Niu, D. Wang, G. Zeng, ACS Appl. Mater. Interfaces 8 (2016) 32887–32900.
[44] C. Zhang, C. Lai, G. Zeng, D. Huang, L. Tang, C. Yang, Y. Zhou, L. Qin, M. Cheng, Biosens. Bioelectron. 81 (2016) 61–67.
[45] W. Iqbal, C. Dong, M. Xing, X. Tan, J. Zhang, Catal. Sci. Technol. 7 (2017) 1726–1734.
[46] C. Liu, Y. Zhang, F. Dong, A.H. Reshak, L. Ye, N. Pinna, C. Zeng, T. Zhang, H. Huang, Appl. Catal. B: Environ. 203 (2017) 465–474.
[47] S. Guo, Z. Deng, M. Li, B. Jiang, C. Tian, Q. Pan, H. Fu, Angew. Chem. Int. Ed. 55 (2016) 1830–1834.
[48] Y. Yao, H. Chen, J. Qin, G. Wu, C. Lian, J. Zhang, S. Wang, Water Res. 101 (2016) 281–291.
[49] Y. Deng, L. Tang, G. Zeng, Z. Zhu, M. Yan, Y. Zhou, J. Wang, Y. Liu, J. Wang, Appl. Catal. B: Environ. 203 (2017) 343–354.
[50] J. Zhang, X. Chen, K. Takanabe, K. Maeda, K. Domen, J.D. Epping, X. Fu, M. Antonietti, X. Wang, Angew. Chem. Int. Ed. 49 (2010) 441–444.
[51] Y.-S. Jun, E.Z. Lee, X. Wang, W.H. Hong, G.D. Stucky, A. Thomas, Adv. Funct.

Mater. 23 (2013) 3661–3667.
[52] M. Shalom, S. Inal, C. Fettkenhauer, D. Neher, M. J. Am. Chem. Soc. 135 (2013) 7118–7121.
[53] Q. Zheng, D.P. Durkin, J.E. Elenewski, Y. Sun, N.A. Banek, L. Hua, H. Chen, M.J. Wagner, W. Zhang, D. Shuai, Environ. Sci. Technol. 50 (2016) 12938–12948.
[54] M. Peer, M. Lusardi, K.F. Jensen, Chem. Mater. 29 (2017) 1496–1506.
[55] X. Wang, K. Maeda, A. Thomas, K. Takanabe, G. Xin, J.M. Carlsson, K. Domen, M. Antonietti, Nature Mater. 8 (2009) 76–80.
[56] P. Yang, H. Ou, Y. Fang, X. Wang, Angew. Chem. Int. Ed. 56 (2017) 3992–3996.
[57] S. Guo, Z. Deng, M. Li, B. Jiang, C. Tian, Q. Pan, H. Fu, Angew. Chem. Int. Ed. 55 (2016) 1830–1834.
[58] M. Shalom, M. Guttentag, C. Fettkenhauer, S. Inal, D. Neher, A. Llobet, M. Antonietti, Chem. Mater. 26 (2014) 5812–5818.
[59] S. Yan, Z. Li, Z. Zou, Langmuir 25 (2009) 10397–10401.
[60] L. Lin, H. Ou, Y. Zhang, X. Wang, ACS Catal. 6 (2016) 3921–3931.
[61] K. Schwinghammer, M.B. Mesch, V. Duppel, C. Ziegler, J.R. Senker, B.V. Lotsch, J. Am. Chem. Soc. 136 (2014) 1730–1733.
[62] S. Yan, Z. Li, Z. Zou, Langmuir 26 (2010) 3894–3901.
[63] J. Zhang, F. Huang, Appl. Surf. Sci. 358 (2015) 287–295.
[64] S. Panneri, P. Ganguly, M. Mohan, B.N. Nair, A.A.P. Mohamed, K.G. Warrier, U.S. Hareesh, ACS Sustain. Chem. Eng. 5 (2017) 1610–1618.
[65] C. Feng, Z. Wang, Y. Ma, Y. Zhang, L. Wang, Y. Bi, Appl. Catal. B: Environ. 205 (2017) 19–23.
[66] Z. Wan, G. Zhang, X. Wu, S. Yin, Appl. Catal. B: Environ. 207 (2017) 17–26.
[67] F. Chen, Q. Yang, S. Wang, F. Yao, J. Sun, Y. Wang, C. Zhang, X. Li, C. Niu, D. Wang, G. Zeng, Appl. Catal. B: Environ. 209 (2017) 493–505.
[68] Y. Shang, X. Chen, W. Liu, P. Tan, H. Chen, L. Wu, C. Ma, X. Xiong, J. Pan, Appl. Catal. B: Environ. 204 (2017) 78–88.
[69] F. Chen, Q. Yang, Y. Zhong, H. An, J. Zhao, T. Xie, Q. Xu, X. Li, D. Wang, G. Zeng, Water Res. 101 (2016) 555–563.